Laser Desorption Ionization Mass Spectrometry on Silicon Nanowell Arrays

ARTICLE *in* ANALYTICAL CHEMISTRY · SEPTEMBER 2010

Impact Factor: 5.64 · DOI: 10.1021/ac101149b · Source: PubMed

7 AUTHORS, INCLUDING:

Basri Gulbakan
Hacettepe University
12 PUBLICATIONS **345** CITATIONS
SEE PROFILE

Dooho Park
Samsung Electro-Mechanics
3 PUBLICATIONS **29** CITATIONS
SEE PROFILE

Kaan Kececi
Istanbul Medeniyet Universitesi
10 PUBLICATIONS **162** CITATIONS
SEE PROFILE

Weihong Tan
University of Florida
573 PUBLICATIONS **28,474** CITATIONS
SEE PROFILE

Published in final edited form as:
Anal Chem. 2010 September 15; 82(18): 7566–7575. doi:10.1021/ac101149b.

LASER DESORPTION IONIZATION MASS SPECTROMETRY ON SILICON NANOWELL ARRAYS

Basri Gulbakan[1,2,3,*], **Dooho Park**[1,2,*], **Myungchan Kang**[1,2], **Kaan Kececi**[1,2], **Charles R. Martin**[1,2], **David H. Powell**[1,4], and **Weihong Tan**[1,2,3]

[1] Department of Chemistry, University of Florida, Gainesville, FL

[2] Center for Research at the Bio/Nano Interface

[3] Shands Cancer Center and UF Genetics Institute

[4] UF Metabolomics Core

Abstract

This paper describes a new technique for fabrication of nanostructured porous silicon (pSi) for laser desorption ionization mass spectrometry. Porous silicon nanowell arrays were prepared by argon plasma etching through an alumina mask. Porous silicon prepared in this way proved to be an excellent substrate for desorption/ionization on silicon (DIOS) mass spectrometry (MS) using adenosine, Pro-Leu-Gly tripeptide and [Des-Arg^9]-bradykinin as the model compounds. It also allows the analyses of complex biological samples such as a tryptic digest of bovine serum albumin, and a carnitine standard mixture. Nanowell array surfaces were also used for direct quantification of the illicit drug fentanyl in red blood cell extracts. This method also allows full control of the surface features. MS results suggested that the pore depth has significant effect on the ion signals. Significant improvement in the ionization was observed by increasing the pore depth from 10 nm to 50 nm. These substrates are useful for laser desorption ionization in both the atmospheric pressure and vacuum regimes.

INTRODUCTION

Matrix-assisted laser desorption/ionization (MALDI) has been utilized in the study of large biomolecules, such as peptides, proteins, carbohydrates and DNA[1]. The broad success of MALDI-MS is related to the ability of the matrix to incorporate and transfer energy to an analyte, thereby ionizing it in a very soft manner[2–4]. However, MALDI is complicated because the presence of the matrix often causes heterogeneous co-crystallization of the matrix and analyte, resulting in significant background ion intensity in the low-mass range (<500 *m/z*)[1, 5–7].

As a complementary alternative, Siuzdak and co-workers have developed desorption/ionization on silicon (DIOS) using nanoporous silicon substrates for the detection of small peptides and antiviral drugs without any mass interference due to matrix ions[6, 8, 9]. In DIOS-MS, the analytes in solution are directly deposited on a nanoporous silicon surface without a chemical matrix. Compared to MALDI, this approach provides simplified sample preparation, more uniform surfaces, and less background noise at masses below 600 Da. Although the DIOS mechanism is not fully understood, porous silicon was found to be an effective medium for desorbing compounds and generating intact ions in the gas phase[6, 9,

Corresponding author, tan@chem.ufl.edu.
*These authors contributed equally to this study.

[10]. It is suggested that porous silicon effectively absorbs and transfers the energy from the UV irradiation laser to the adsorbed analytes, while also protecting these molecules from fragmentation caused by direct laser exposure[10, 11].

Most existing DIOS platforms are prepared by electrochemical anodization of crystalline silicon, necessitating the use of toxic HF solution[12]. In addition, it is difficult to obtain reproducible surfaces with the same nanostructures, because pore size and pore density are not well controlled by chemical etching[7, 13]. To overcome this issue, Vertes et.al reported the use of silicon microcolumn arrays and silicon nanopost arrays as alternative DIOS substrates and showed that structure specific fragmentation can also be induced.[14, 15, 16]. In another study He et al. have used electron beam lithography (EBL) [7] and nanosphere lithography[17] to investigate the impact of the surface morphology of porous silicon on analyte desorption and ionization. Electron beam lithography allows accurate fabrication of sub-100 nm features, but the serial nature of the technique makes it very slow. In the nanosphere technique, the self-assembly can be very time consuming, and long-range order is still not achieved[18].

Self-ordered porous alumina substrates have also been used as useful platforms for laser desorption/ionization MS[19–21]. Because Wada et al. found that surface electroconductivity was one of the requirements for a porous alumina chip to be effective for laser-induced desorption/ionization, the surface was coated with gold or platinum[20]. Masuda et al. suggested that the porous alumina layer beneath the surface metal probably acted as a thermal insulator[21].

In this paper, we report the fabrication of porous silicon by a non-lithographic method using a self-ordered porous alumina membrane and subsequent application for laser desorption ionization mass spectrometry. The self-ordered pore pattern of the alumina membrane is transferred into the silicon substrate via a plasma-etching method, resulting in rapid, low cost and reproducible fabrication without the use of toxic chemicals. Pore size and porosity are comparable to that of the alumina mask and the pore depth can be controlled in the range of 10 nm to 50 nm by changing the etch time. The porous silicon platforms with 10 nm, 30 nm and 50 nm-depth nanowells were used for laser desorption/ionization (LDI) MS detection of biomolecules. To the best of our knowledge, laser desorption ionization at this depth regime has not been reported previously, and the submicrometer porosity limit to induce ionization is yet unclear. The utility of nanowell arrays under atmospheric pressure and vacuum regimes was also studied.

EXPERIMENTAL

Materials

Aluminum foil (99.99%) was obtained from Alfa Aesar. Single-side polished P/Boron type silicon wafers, having {100} orientation, low resistivity (0.01–0.02 Ω cm), 525 ± 25 μm thickness and 100 mm diameter were obtained from Silicon Valley Microelectronics, Inc. (Santa Clara, CA). Phosphoric acid, sulfuric acid, chromium trioxide, oxalic acid and hydrogen peroxide were obtained from Fisher Scientific. Triton X-100, adenosine, Pro-Leu-Gly tripeptide and [*Des-Arg*^{9}]-bradykinin were obtained from Sigma-Aldrich. Stock solutions (500 pmol/μL) of these analytes were prepared by dissolving each compound in 1:1 acetonitrile:aqueous 0.1 % trifluoroacetic acid solution. Bovine serum albumin (BSA) was obtained from Sigma-Aldrich. In-Solution tryptic digestion and guanidination Kit was obtained from Pierce, and digestion of 10 μg of BSA was carried out using the manufacturer's instructions. A carnitine metabolite cocktail containing carnitine, butyrylcarnitine, octanoylcarnitine decanoylcarnitine, myristoylcarnitine, palmitoylcarnitine, stearoylcarnitine (5 ppm each) and red blood cell extracts were provided by Dr. Peggy

Borum (University of Florida) as a kind gift and used without any further treatment. A reference standard solution of fentanyl (1.0 mg/mL in methanol) was obtained from Restek and used with further dilution in methanol.

Preparation of porous alumina mask

The alumina mask was an inhouse-prepared nanopore alumina film. The electrochemical anodization method used to prepare these films has been described previously[22]. The same procedure was followed for preparation of the alumina masks.

Fabrication of the nanowell arrays on silicon substrates

Silicon wafers were cleaned in a piranha solution (3:1 (v/v) 98% H_2SO_4: 30% H_2O_2) for 30 min. The silicon substrates were rinsed with deionized water, followed by drying under a stream of nitrogen. The alumina mask was mounted on top of the silicon wafer with the barrier-layer side of the mask facing up using a drop of Triton X-100 solution as an adhesive. The masked substrate was then inserted into the vacuum chamber of a reactive-ion etching apparatus (Samco® model RIE-1C). Argon plasma was used to etch the substrate surface through the mask with the following etching parameters: 13.56 MHz, 100 W, 10 Pa, 12 sccm Ar flow. The etch time was varied (5, 10, 15, 20, and 25 mins, respectively) in order to determine the etch rate of silicon under these conditions. The alumina mask was removed by the use of sonication in water for 10 min. The silicon substrates were rinsed with nanopure water and ethanol followed by drying with a stream of nitrogen gas. Porous silicon substrates were stored in ethanol and they were redried by N_2 flow just prior to mass spectrometry experiments.

Fabrication of desorption/ionization on silicon (DIOS) surfaces—To provide a benchmark for comparison, standard DIOS surfaces have been prepared following the previously reported method[5]. Briefly, low resistivity (0.01–0.02 Ω cm) silicon wafers were sputter-coated with 30-Å Au with an a Desk II Cold Sputter instrument (Denton Vacuum, LLC) and chemically etched using the HOME method with a solution of 1:1:2 EtOH/HF (49%)/H_2O_2 (30%) for 30 s.

Characterization of porous surfaces

Tapping mode Atomic Force Microscopy (AFM) was used to examine the morphology and depth of the nanowell-array-on-silicon substrates. In order to investigate the etch rate, three porous silicon samples were prepared at each etch time. The average depth of wells (at least 450 nanowells) for each etching time was obtained from three different positions of each sample. AFM experiments were performed using a Multimode AFM with a NanoScope IIIa controller (Digital Instruments, Santa Barbara, CA) and MPP-11200 Si tips (Veeco, manufacturer's suggested tip radius is $r < 10$ nm). Height images were obtained in the tapping mode under dry N_2 gas. The nanowell depth was assessed using the profile analysis made by the WSxM image analysis package (Nanotec Electronica, Madrid, Spain).

A Hitachi S4000 FE-SEM was used to obtain the pore diameter and the thickness of the alumina mask. Both the top view and the cross section of the alumina membrane were investigated. All samples were coated with an Au/Pd film by a Desk II Cold Sputter instrument (Denton Vacuum, LLC).

Mass Spectrometry

Mass spectra were acquired using an Agilent 6210 MSD time-of-flight (TOF) mass spectrometer configured for ESI (Agilent Technologies Inc., Santa Clara, CA, USA). Laser desorption/ionization experiments were conducted by installing an external MassTech

atmospheric pressure/matrix assisted laser desorption ionization pulse dynamic focusing (AP/MALDI PDF) ion source. The results were analyzed using Analyst® software. Mass spectrometry experiments in the vacuum regime were conducted using an ABI 4700 MALDI TOF-TOF proteomics analyzer (Applied Biosystems, Framingham, MA) equipped with an Nd:YAG laser (355 nm, 3–7 ns pulses) which was operated in the reflector, positive ion mode with an acceleration voltage of 20 kV. The laser was operated at a fixed fluence at 200 Hz. The laser-firing pattern was set to "uniform." Both the sample plate and the laser were aligned before spectral acquisition. Spectra were smoothed by "noise filter" and baseline corrected with Data Explorer 4.0.

RESULTS AND DISCUSSION

Characterization of porous silicon substrates

Characterization of alumina mask—Figure 1 shows representative SEM images of the mask prepared as described in an earlier publication[22]. The pores were formed in a hexagonally packed array (Figure 1A). Image J software (Wayne Rasband, NIH, USA) was used to characterize the morphology of the alumina membrane: pore diameter (80 ± 5 nm); pore density ((9.3 ± 0.3) × 10^9 pores/cm^2); porosity (48 ± 2 %). These films have two distinct surfaces. Figure 1A shows the surface that faced the solution during the anodization, while Figure 1B shows the surface that faced the Al substrate during the anodization. The latter surface is often called the "barrier layer," because it initially has a film coating which must be removed during processing. In Figure 1C the cross section of the film indicates that the thickness was 2.3 μm and that the pores were cylindrical.

Fabrication and morphology of porous silicon substrates—In Figure 2, AFM images show the surface characteristics of the silicon nanowell-array: density (6.0×10^9 nanowells/cm^2), diameter (93±7 nm), and porosity (44%). According to surface characteristics from AFM images, the pore pattern of the alumina mask was successively transferred into silicon substrates. The pore size, pore density and porosity of porous silicon are compatible to those of the alumina mask. The pore diameter showed a narrow distribution. Moreover, as shown in Figure 3, as the etching time was increased, the depth of nanowells increased linearly while the array pattern remained unchanged.

Mass spectrometry analyses

Porous silicon substrates were prepared by etching for 5 min (depth = 10 nm) and 15 min (depth = 30 nm) and 25 min (depth = 50 nm). Silicon nanowells were spotted with 0.2 μL of 5 pmol/μL solutions of adenosine, Pro-Leu-Gly tripeptide and bradykinin, and the samples were dried in room temperature for 30 mins prior to analyses. For comparison of atmospheric pressure laser desorption versus vacuum laser desorption, 0.2 μL of 500 pmol/μL solutions of the respective analytes were used. A schematic of the entire process is shown in Figure 4.

The mass spectra of adenosine acquired on 10 nm, 30 nm, 50 nm nanowell surfaces (Figure 5) and the DIOS surface clearly show that an increase in etching time provides a significant improvement in the ion signal. Analyses with the 10 nm-deep pores were repeated with concentrations from 1 pmol to 500 pmol and with various laser attenuations, but no significant improvement was observed. In a recent report on the thermochemistry of adenosine[23], it was shown that a significant amount of energy has to be imparted to induce protonation. The authors reported the proton affinity of adenosine as 979 ± 1 kJ/mol in the gas-phase using nano-ESI-MS. In the light of these findings, we can hypothesize that for the surface etched to a depth of 10 nm, the surface induced heating does not provide sufficient energy to desorb the molecule from the surface and ionize it. However, when the etching

time was increased and the same experiment was conducted using 30 nm and 50 nm deep nanowells and the DIOS surface, significant ion signals for protonated adenosine $[M+H]^+$ before (268.1054) and adenine after (136.0594) loss of the ribose group were observed.

After this experiment, analyses on the nanowell surfaces were extended to two different compounds: Pro-Leu-Gly ($[M+H]^+$= 285.1921) and [Des-Arg^9]-bradykinin(($[M+H]^+$= 904.4691). Similar to adenosine, 0.2 μL of 5 pmol/μL of Pro-Leu-Gly and [Des-Arg^9]-bradykinin were spotted on the nanowells and the attenuation of the laser was fixed. The mass spectra are shown in Figures 6 and 7.

The mass spectra for the two compounds clearly show that the ion signals significantly increase with increasing pore depth. Furthermore the electrochemically etched DIOS surface gave higher intensities in all analyses. DIOS surfaces were well characterized previously and have surface features with depths of 200 nm[24] This result led us to think about the events associated with laser desorption/ionization and the effect of increased nanostructuring on the ion signals. Northen et al.[24] reported that the surface area is the key factor. However, Alimpiev et al.[25] demonstrated that the submicrometer surface porosity, irrespective of the substrate material, is the most important effect for desorption/ionization. In the most similar report to our work, Okuno et al.[20] demonstrated that silicon wafers roughened with sandpaper can act as a surface for laser desorption. An increase in surface porosity enhances ion signals via multiple effects: The surface is resupplied with analyte after a laser pulse, and a local environment for the laser-induced field is provided to facilitate physical separation of preformed analyte ions from their counterions. Also, the heat capacity and heat conductivity are decreased when rapid heating of the surface occurs, resulting in effective sublimation of analytes by laser irradiation, as well as effective absorption of the laser light. Recently Hsu et al. [13] showed that laser desorption/ionization can occur even on metals. They showed that although ion signals greatly improve with surface roughness, ionization can occur even on a commercial non-porous aluminum film. Our results are in good agreement with these previous findings. In addition to the unique energy absorbing properties of porous surfaces, nanostructuring also helps to create a thin layer when analytes are spotted and thereby the interaction between the surface and analyte is facilitated resulting in more efficient ionization. This fact has been shown by Finnskoget.al [30] and very recently by Chen et.al.[31]

Significant dimer and trimer signals are observed in Figures 6 and 7. Since the ionization event occurs at atmospheric pressure, it is possible that ion-ion reactions occur after the desorption event, and that dimerization and trimerization are favored. Desorption ionization on porous silicon is mostly carried out in MALDI instruments operating under vacuum, and only a few reports exist about atmospheric pressure DIOS and to date no comparison exists. Since the concentrations of the analyte solutions are low, dimer and trimer formation is probably not due to concentration effects. To investigate this factor, a vacuum MALDI instrument was used both to check the effectiveness of the surfaces in vacuum conditions and to make a comparison between atmospheric pressure and vacuum MALDI regimes. Comparison of atmospheric pressure and vacuum spectra, shown in Figure 8, indicates that a significant difference exists between atmospheric pressure and vacuum regimes. Because the dimer and trimer signals did not appear in vacuum regime, these peaks were due in part to atmospheric pressure conditions.

Application of the nanowell arrays for complex biological mixture analysis

After investigating the ionization efficiencies with increasing pore depth, the nanowell array surfaces were applied to analyses of real biological samples. Carnitines serve as important biomarkers for metabolic disorders and there is a growing interest in the analysis of carnitines in complex biological samples[27,28]. Because of the much larger signal-to-noise

ratios, the nanowells with 50 nm pores were used for these measurements. For this purpose, 0.2 μL of the standard carnitine metabolite cocktail (containing 5 ppm of each component) was spotted on the surfaces. Theoretical masses of the carnitines are given in Table 1. Figure 9 clearly shows that the carnitine standard can be successfully analyzed with a very clean background and no interfering peaks, which are the major drawbacks of the use of MALDI for metabolomics. A tryptic digest of bovine serum albumin (0.2 μL of 5 pmol/μL) was then analyzed on 50 nm deep nanowells, as shown in Figure 10. Many of the tryptic peptides were observed, and it is noteworthy that no peak was observed in the low mass range.

To further demonstrate the analytical applicability of nanowell arrays varying concentrations of the illicit drug fentanyl $[M+H]^+$= 307.2220 (ranging from 200 ng/mL to 1.5 μg/mL) were spiked into a red blood cell extract. The samples were applied to the surfaces using Z-touch method[29] and then analyzed. Figure 11 shows spiked fentanyl in red blood cell extract (200 ng/mL) and the corresponding calibration curve. As can be seen in these data, the nanowell surfaces show good linearity for the analysis of fentanyl in this complex biological mixture.

CONCLUSION

The applicability of nanowell silicon substrates for desorption/ionization on silicon mass spectrometry has been demonstrated. The pore pattern of an alumina mask has been successively transferred onto silicon substrates by means of Ar-ion-plasma etch. This method has several advantages: (1) elimination of toxic HF from the procedure; (2) reproducibility (uniform pore size, pore density, and porosity); and (3) low-cost and rapid production. Nanowell depth is linearly related to etch time. The etch rate was determined to be 2.0 nm/min with about 2 μm thick AAO mask. The pore depth requirement for inducing laser desorption ionization has not been well addressed before and our results show that very little porosity (10 nm) is sufficient to induce ion formation, and that the ion signals significantly improve with increasing pore depth. The results showed that a reasonable level of sensitivity can be achieved with 50 nm deep nanowells. Comparison of nanowell arrays and DIOS surfaces show that ionization is more favored with nanostructures having deeper pores. However, ionization occurs even with a slightly nanostructured surface (10 nm deep nanowells.)

The mechanism of ion formation on nanowell arrays is still not clear but we attribute the ion formation to the unique thermal and optical properties of silicon. We are in the process of systematically investigating the effects of pore size, pore depth and pore density by changing the AAO mask and by controlling the aspect ratio of the nanowells using different substrates. Our initial findings suggest that nanowell arrays are suitable substrates for laser desorption/ionization of biomolecules and can be used for the analysis of small molecules, metabolites and peptides.

Supplementary Material

Refer to Web version on PubMed Central for supplementary material.

Acknowledgments

We are thankful to University of Florida proteomics core facility for providing access to MALDI-TOF/TOF instrument and also to Noelle Elliot and Dr. Peggy Borum at Food Science and Human Nutrition Department for providing carnitine standard and red blood cell extract. This work is supported by NIH grants.

References

1. Hillenkamp F, Karas M, Beavis RC, Chait BT. Analytical Chemistry. 1991; 63:1193A–1203A. [PubMed: 1897719]
2. Dreisewerd K. Chemical Reviews. 2003; 103:395–425. [PubMed: 12580636]
3. Karas M, Kruger R. Chemical Reviews. 2003; 103:427–439. [PubMed: 12580637]
4. Knochenmuss R, Zenobi R. Chemical Reviews. 2003; 103:441–452. [PubMed: 12580638]
5. Kruse RA, Li X, Bohn PW, Sweedler JV. Analytical Chemistry. 2001; 73:3639–3645. [PubMed: 11510828]
6. Lewis WG, Shen ZX, Finn MG, Siuzdak G. International Journal Of Mass Spectrometry. 2003; 226:107–116.
7. Xiao Y, Retterer ST, Thomas DK, Tao JY, He L. The Journal of Physical Chemistry C. 2009; 113:3076–3083.
8. Thomas JJ, Shen Z, Crowell JE, Finn MG, Siuzdak G. Proceedings of the National Academy of Sciences of the United States of America. 2001; 98:4932. [PubMed: 11296246]
9. Wei J, Buriak JM, Siuzdak G. Nature. 1999; 399:243. [PubMed: 10353246]
10. Shen ZX, Thomas JJ, Averbuj C, Broo KM, Engelhard M, Crowell JE, Finn MG, Siuzdak G. Analytical Chemistry. 2001; 73:612–619. [PubMed: 11217770]
11. Zhan Q, Wright SJ, Zenobi R. Journal Of The American Society For Mass Spectrometry. 1997; 8:525–531.
12. Shenar N, Martinez J, Enjalbal C. Journal of the American Society for Mass Spectrometry. 2008; 19:632–644. [PubMed: 18356075]
13. Hsu NY, Tseng SY, Wu CY, Ren CT, Lee YC, Wong CH, Chen CH. Analytical Chemistry. 2008; 80:5203–5210. [PubMed: 18489127]
14. Chen Y, Vertes A. Analytical Chemistry. 2006; 78:5835–5844. [PubMed: 16906730]
15. Walker BN, Razunguzwa T, Powell M, Knochenmuss R, Vertes A. Angewandte Chemie International Edition. 2009; 48:1669–1672.
16. Stolee, JA.; Chen, Y.; Vertes, A. Journal Of Physical Chemistry C. 2009. p. 113http://dx.doi.org/10.1021/jp906834z
17. Finkel NH, Prevo BG, Velev OD, He L. Analytical Chemistry. 2005; 77:1088–1095. [PubMed: 15858990]
18. Sainiemi L, Keskinen H, Aromaa M, Luosujarvi L, Grigoras K, Kotiaho T, Makela JM, Franssila S. Nanotechnology. 2007; 18:505303.
19. Nayak R, Knapp DR. Analytical Chemistry. 2007; 79:4950–4956. [PubMed: 17547367]
20. Okuno S, Arakawa R, Okamoto K, Matsui Y, Seki S, Kozawa T, Tagawa S, Wada Y. Analytical Chemistry. 2005; 77:5364–5369. [PubMed: 16097781]
21. Wada Y, Yanagishita T, Masuda H. Analytical Chemistry. 2007; 79:9122–9127. [PubMed: 17979256]
22. Li N, Mitchell DT, Lee KP, Martin CR. Journal of the Electrochemical Society. 2003; 150:A979–A984.
23. Touboul D, Bouchoux G, Zenobi R. Journal Of Physical Chemistry B. 2008; 112:11716–11725.
24. Northen TR, Woo HK, Northen MT, Nordstrom A, Uritboonthail W, Turner KL, Siuzdak G. Journal Of The American Society For Mass Spectrometry. 2007; 18:1945–1949. [PubMed: 17881245]
25. Alimpiev S, Nikiforov S, Karavanskii V, Minton T, Sunner J. The Journal of Chemical Physics. 2001; 115:1891–1901.
26. Huikko K, Östman P, Sauber C, Mandel F, Grigoras K, Franssila S, Kotiaho T, Kostiainen R. Rapid communications in mass spectrometry. 2003; 17:1339–1343. [PubMed: 12811757]
27. Jones LL, McDonald DA, Borum PR. Progress in Lipid Research. 2001; 49:61–75. [PubMed: 19720082]
28. Wikoff WR, Gangoitti JA, Barshop BA, Siuzdak G. Clinical Chemistry. 2007; 53(12):2169–2176. [PubMed: 17951291]

29. Northen TR, Yanes O, Northen MT, Marrinucci D, Uritboonthai W, Apon J, Golledge SL, Nordstrom A, Siuzdak G. Nature. 2007; 449(7165):1033–U3. [PubMed: 17960240]
30. Finnskog D, Jaras K, Ressine A, Malm J, Marko-Varga G, Lilja H, Laurell T. Electrophoresis. 2006; 27:1093–1103. [PubMed: 16523454]
31. Chen SY, Li KI, Yu CS, Wang JS, Hu YC, Lai CC. Analytical Chemistry. 201010.1021/ac101426n

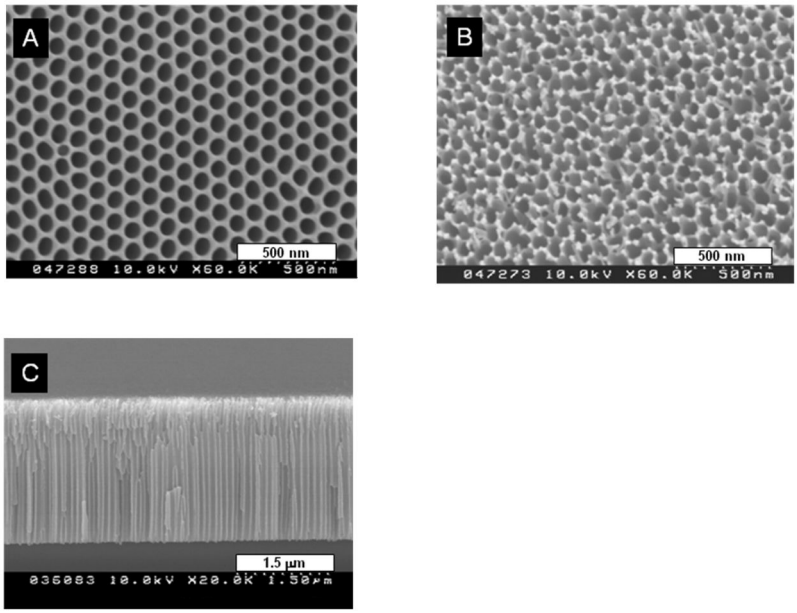

Figure 1.
Scanning electron micrographs of the alumina mask: Top view of (**A**) outer surface and (**B**) barrier layer surface, and (**C**) cross section.

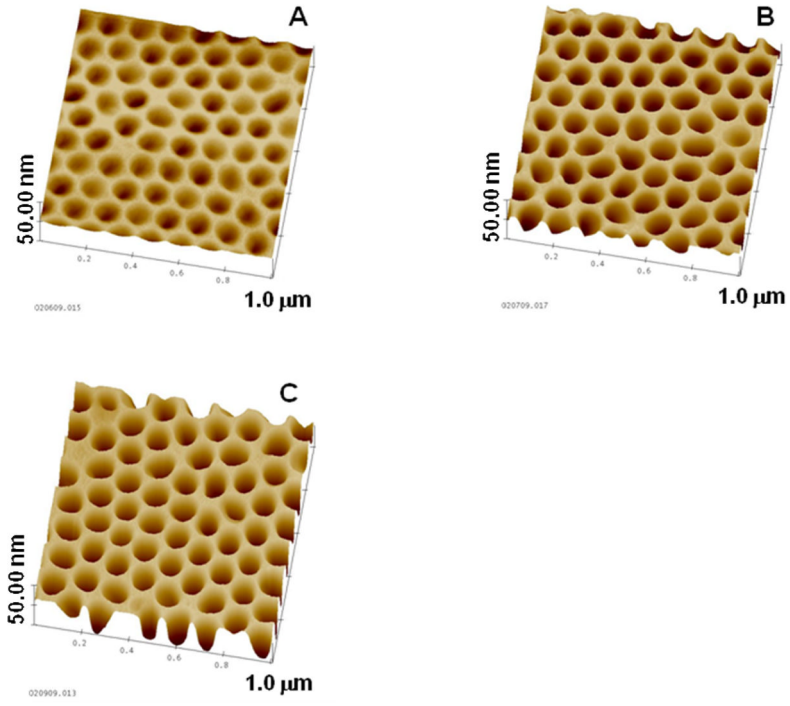

Figure 2.
Tapping mode AFM images of nanowell arrays on silicon substrates prepared by means of Ar-ion plasma etching for: (**A**) 5 mins, (**B**) 15 mins, and (**C**) 25 mins.

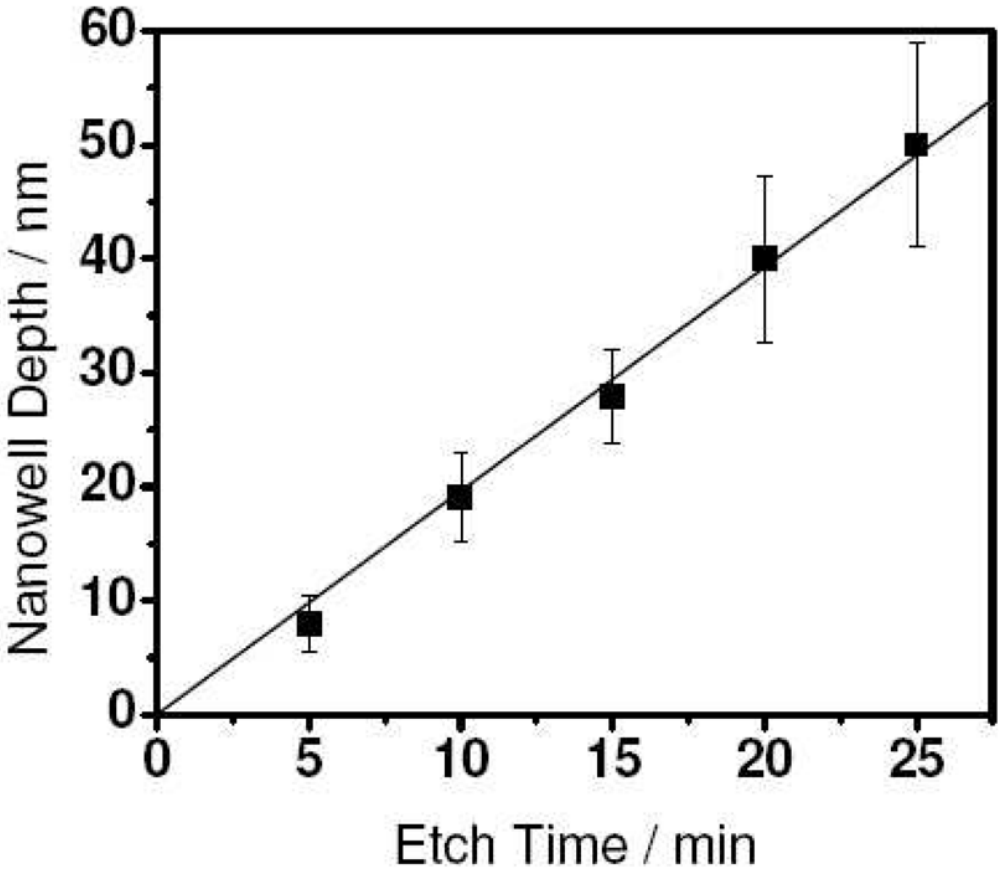

Figure 3.
Nanowell depth vs etch time (The solid line is the linear regression best fit line (slope = 2.0 nm/min; R = 0.99932).

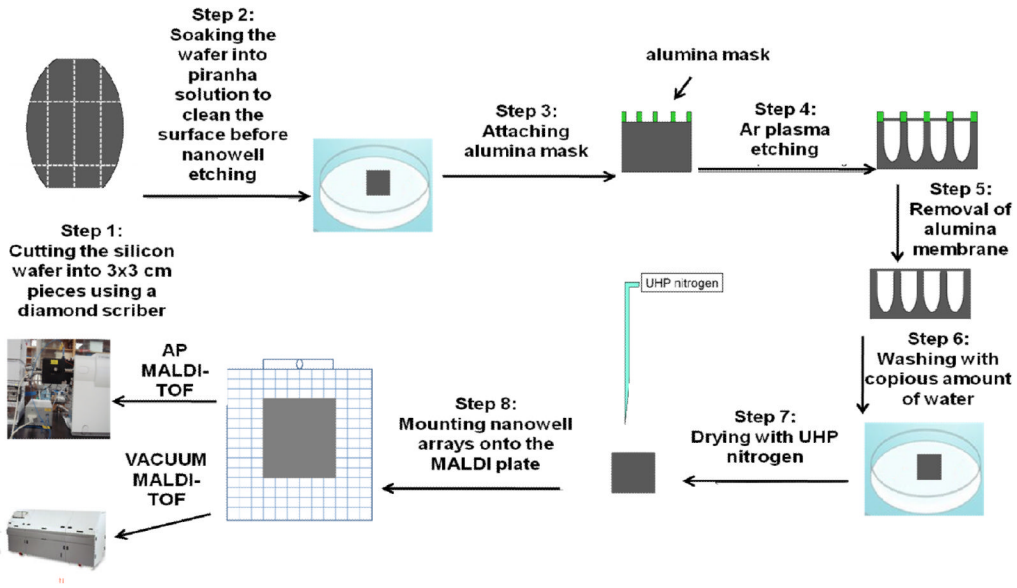

Figure 4.
Workflow for the preparation of nanowell arrays and MS analysis.

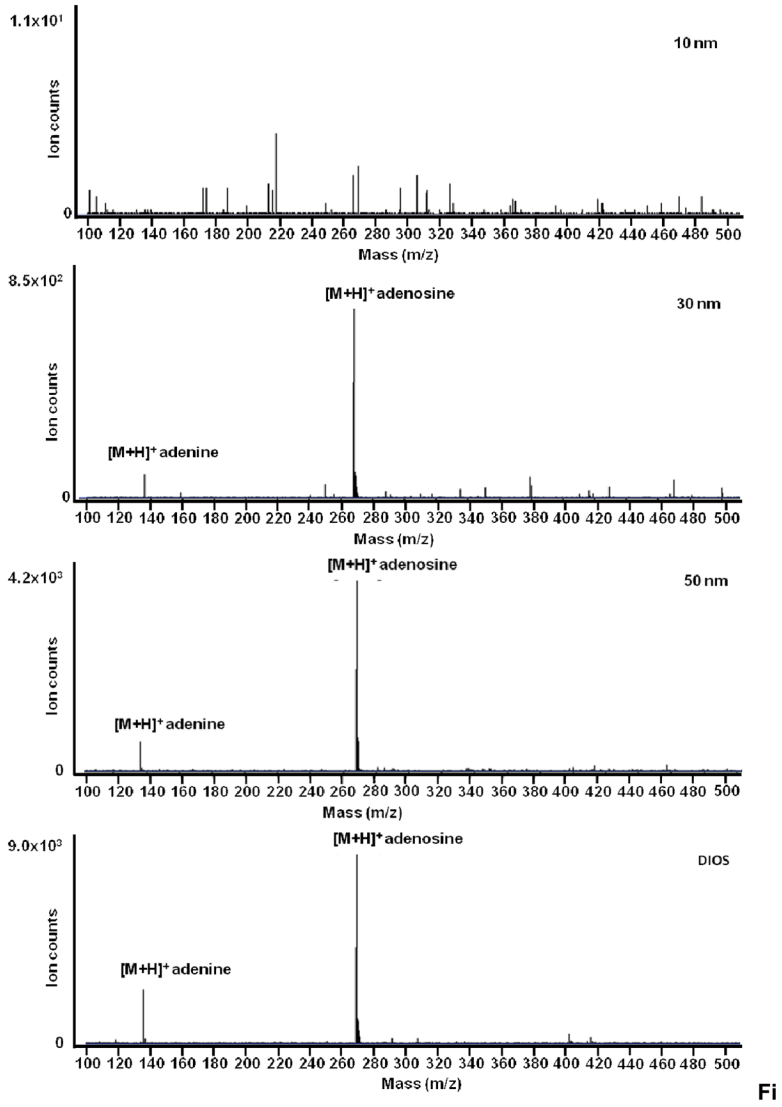

Figure 5.
Mass spectra of adenosine acquired on 10 nm, 30 nm, 50 nm-deep nanowells and a DIOS surface

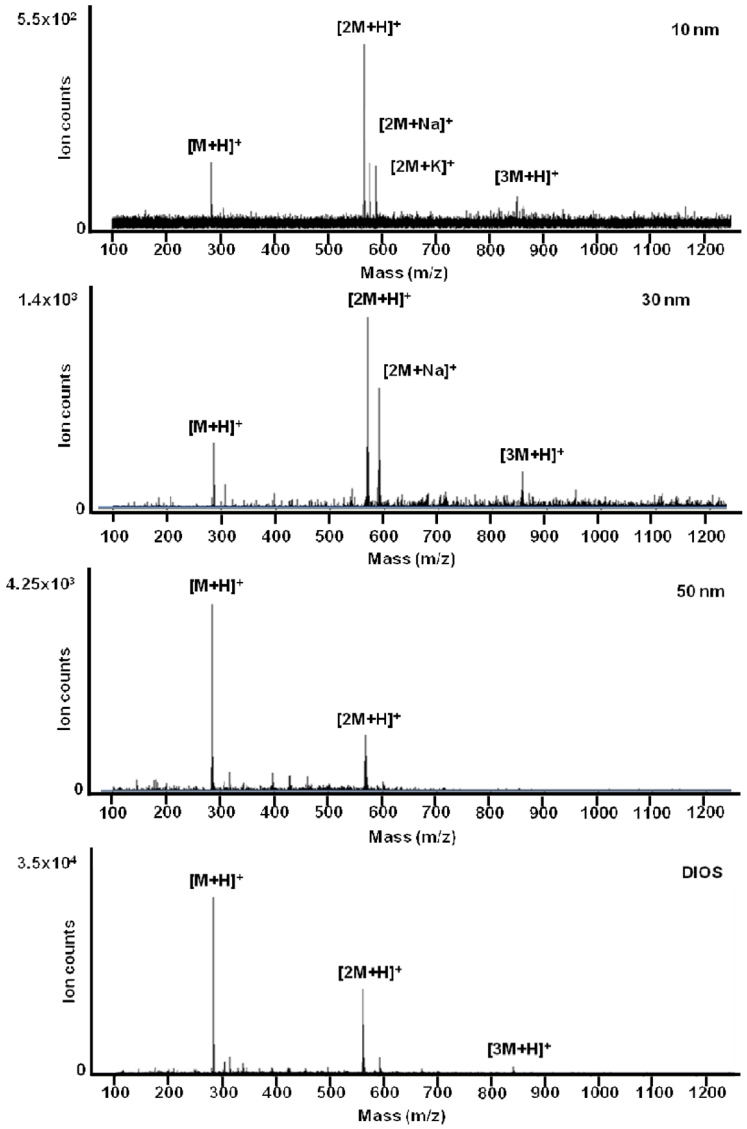

Figure 6.
Mass spectra of Pro-Leu-Gly acquired on 10 nm, 30 nm, 50 nm deep nanowells and DIOS surface

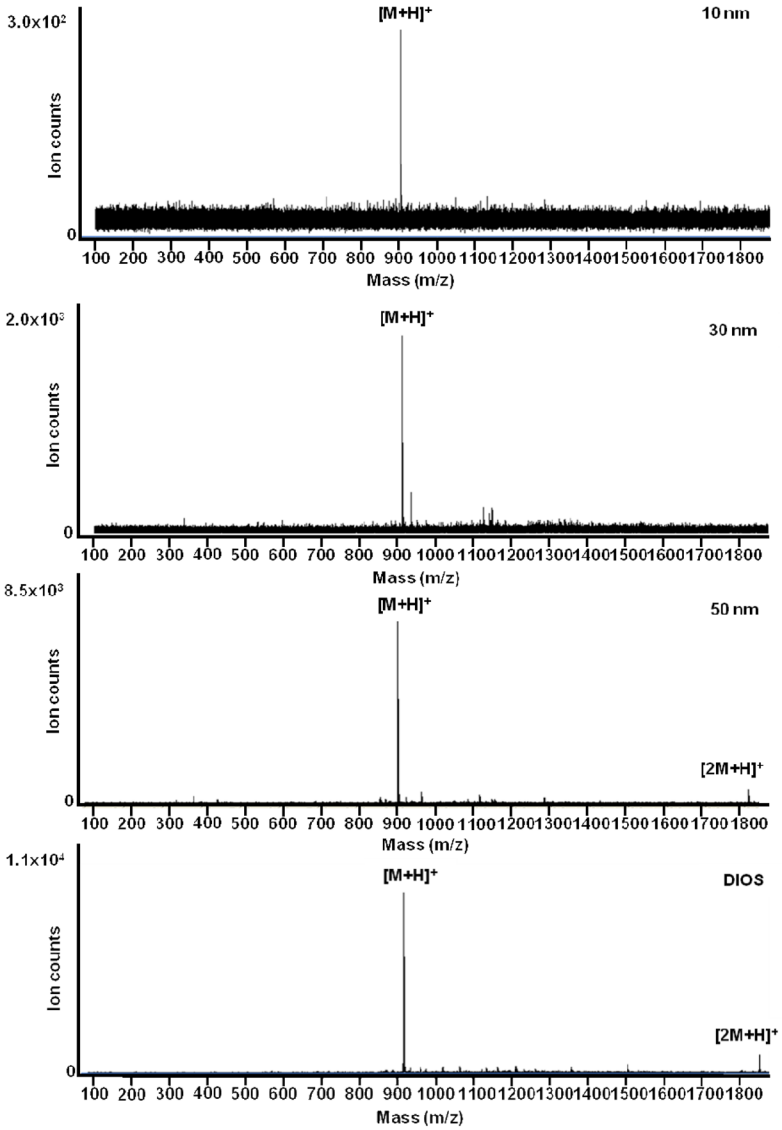

Figure 7.

Mass spectra of [des-Arg^9]-bradykinin, on 10 nm, 30 nm, 50 nm deep nanowells and the DIOS surface

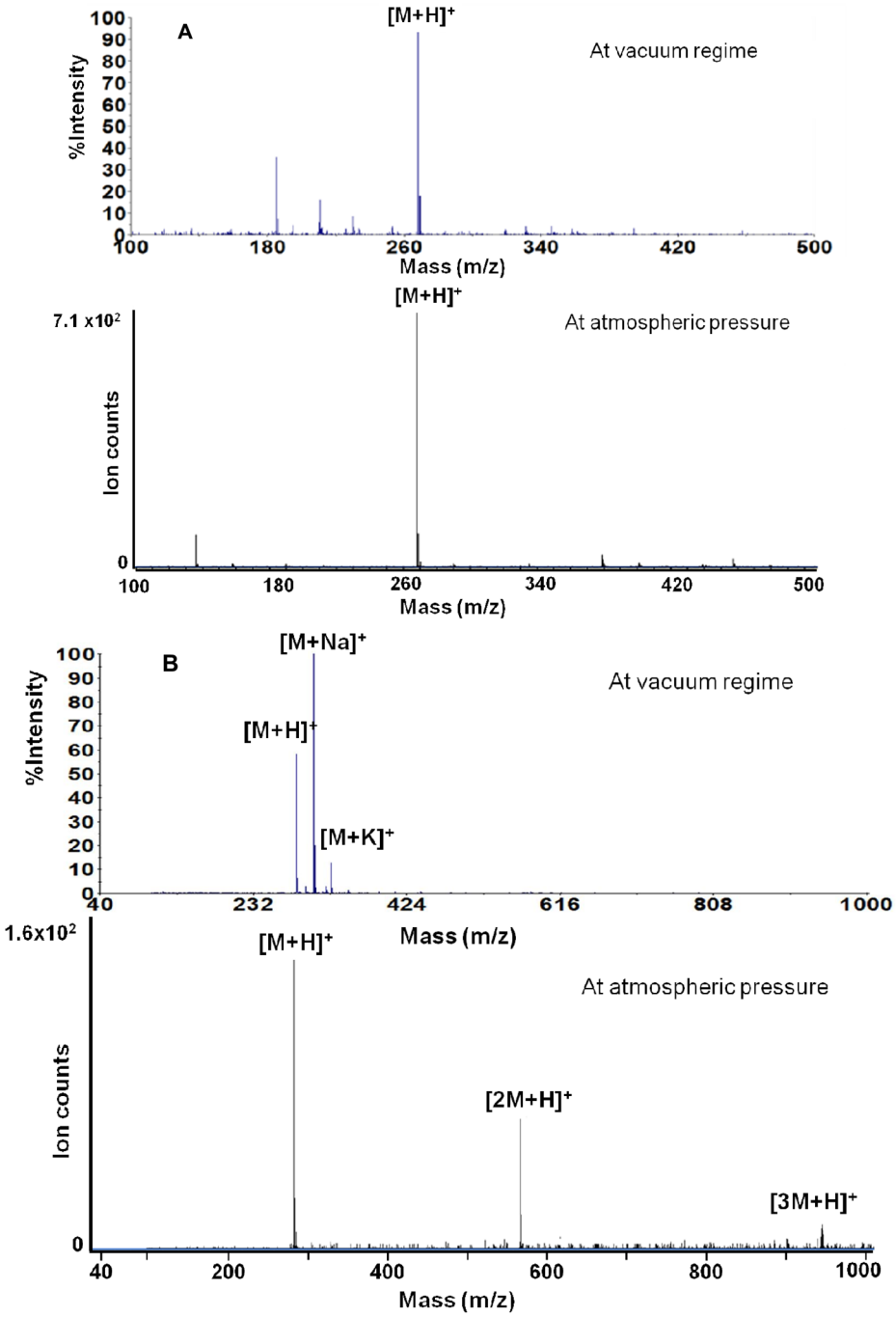

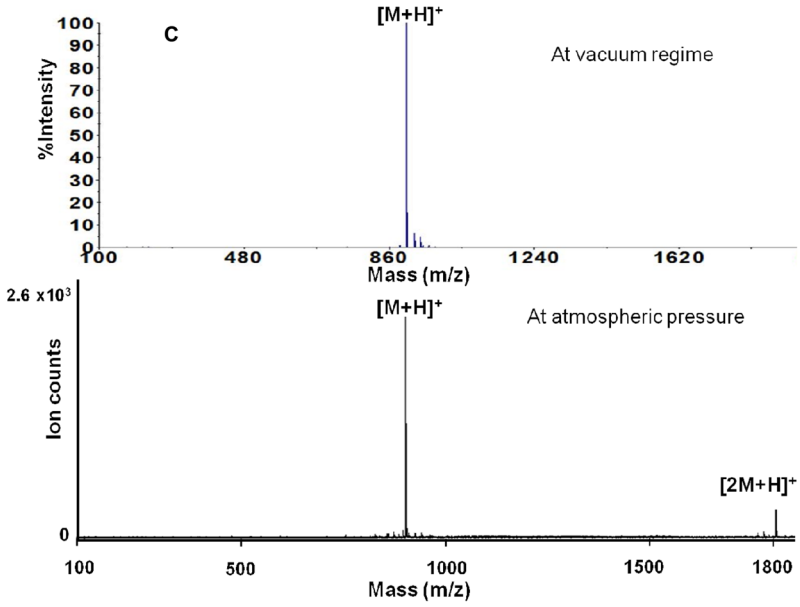

Figure 8.

Comparison of atmospheric pressure and vacuum regime laser desorption ionization on 30 nm-deep nanowell arrays.

A: Adenosine, B: Pro-Leu-Gly, C: [Des-Arg^9]-bradykinin

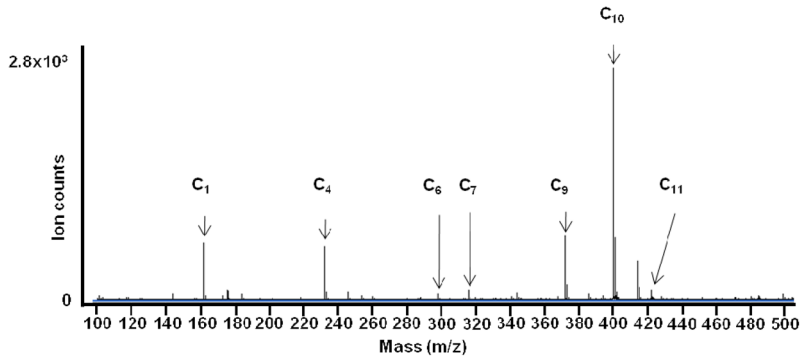

Figure 9.
Analysis of carnitine standard solution on 50 nm deep nanowell array.

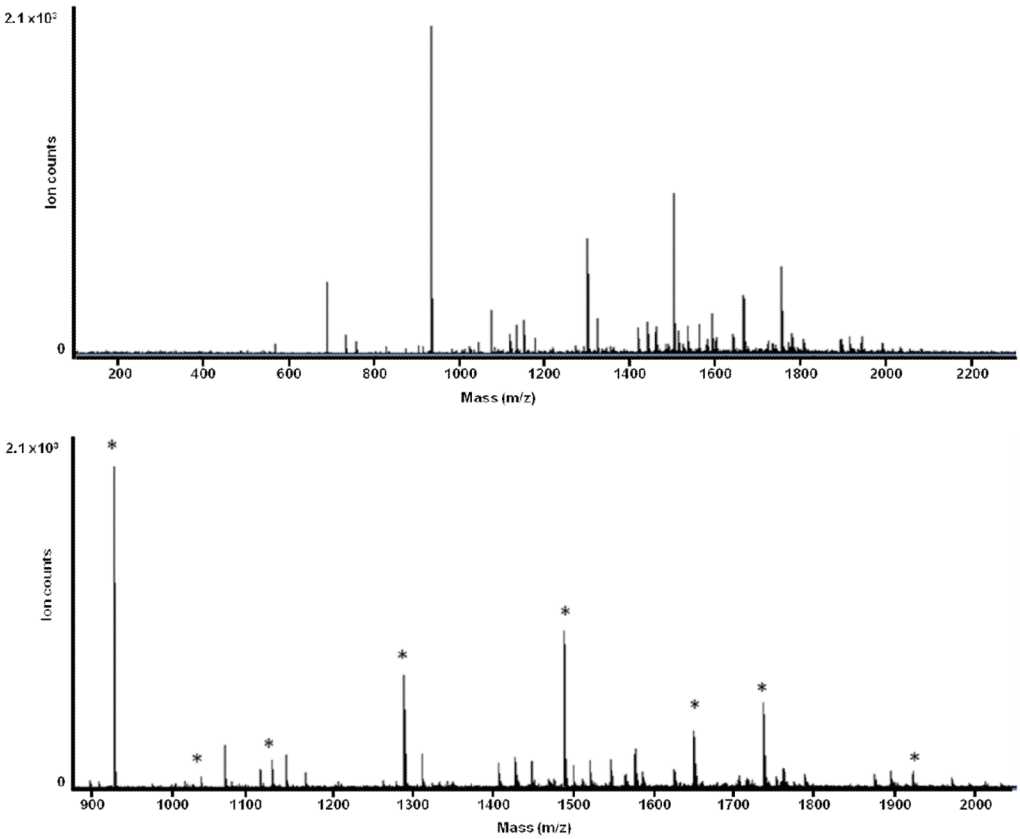

Figure 10.
Analysis of tryptic digest of BSA on a 50 nm deep nanowell array. Peaks labeled with (*) denote tryptic peptides.

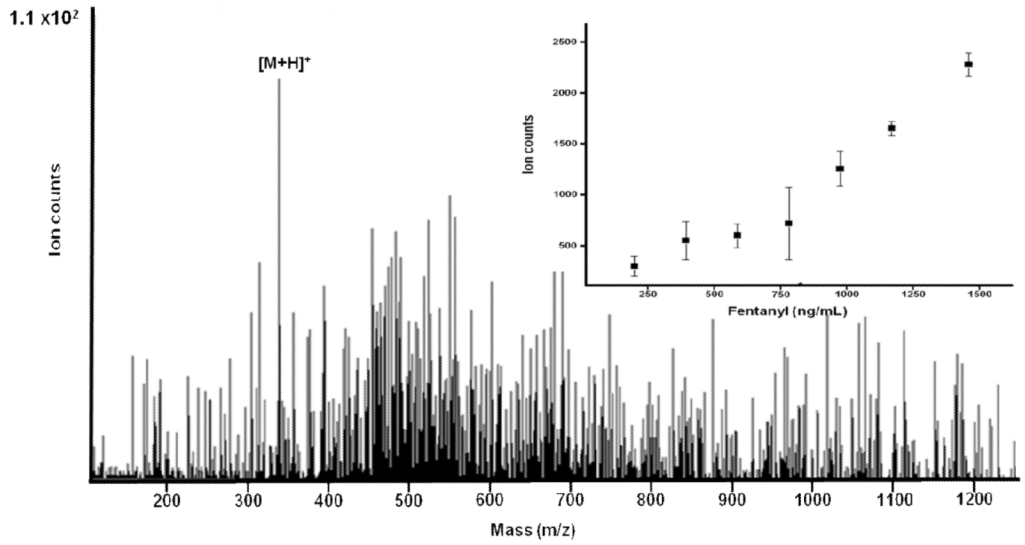

Figure 11.

Mass spectrum of fentanyl in a red blood cell extract (200 ng/mL) obtained on a 50-nm deep nanowell array. Inset shows the calibration curve for fentanyl over the range of 200ng/mL to 1.5 μg/mL.

Table 1

. m/z ratios of the carnitine standards.

Name of the carnitine	$[M+H]^+$ m/z
Carnitine (C1)	162.1125
Butyrylcarnitine (C4)	232.1543
Octanoylcarnitine(C5)	288.2169
Decanoylcarnitine(C6)	316.2482
Myristoylcarnitine(C9)	372.3108
Palmitoylcarnitine(C10)	400.3421
Stearoylcarnitine(C11)	428.3734